Acta Biomaterialia 70 (2018) 35–47

Contents lists available at ScienceDirect

Acta Biomaterialia

journal homepage: www.elsevier.com/locate/actabiomat

Full length article

Nanoengineered injectable hydrogels for wound healing application

Giriraj Lokhande [a], James K. Carrow [a], Teena Thakur [a], Janet R. Xavier [a], Madasamy Parani [a,b], Kayla J. Bayless [d], Akhilesh K. Gaharwar [a,c,e,*]

[a] Department of Biomedical Engineering, Texas A&M University, College Station, TX 77843, United States
[b] Department of Genetic Engineering, SRM University, Chennai, Tamil Nadu 603 203, India
[c] Department of Materials Sciences, Texas A&M University, College Station, TX 77843, United States
[d] Department of Molecular and Cellular Medicine, Texas A&M University Health Science Center, College Station, TX 77843, United States
[e] Center for Remote Health Technologies and Systems, Texas A&M University, College Station, TX 77843, United States

ARTICLE INFO

Article history:
Received 6 November 2017
Received in revised form 15 January 2018
Accepted 29 January 2018
Available online 7 February 2018

Keywords:
Two-dimensional nanoparticles
Nanocomposite hydrogels
Wound healing
Hemostasis
Therapeutic release
Kappa-carrageenan

ABSTRACT

We report injectable nanoengineered hemostats for enhanced wound healing and tissue regeneration. The nanoengineered system consists of the natural polysaccharide, κ-carrageenan (κCA), loaded with synthetic two-dimensional (2D) nanosilicates. Nanoengineered hydrogels showed shear-thinning characteristics and can be injected for minimally invasive approaches. The injectable gels can be physically crosslinked in presence of monovalent ions to form mechanically strong hydrogels. By controlling the ratio between κCA and nanosilicates, compressive stiffness of crosslinked hydrogels can be modulated between 20 and 200 kPa. Despite high mechanical stiffness, nanocomposite hydrogels are highly porous with an interconnected network. The addition of nanosilicates to κCA increases protein adsorption on nanocomposite hydrogels that results in enhance cell adhesion and spreading, increase platelets binding and reduce blood clotting time. Moreover, due to presence of nanosilicates, a range of therapeutic biomacromolecules can be deliver in a sustain manner. The addition of nanosilicates significantly suppresses the release of entrap vascular endothelial growth factor (VEGF) and facilitate *in vitro* tissue regeneration and wound healing. Thus, this multifunctional nanocomposite hydrogel can be used as an injectable hemostat and an efficient vehicle for therapeutic delivery to facilitate tissue regeneration.

Statement of Significance

Hemorrhage is a leading cause of death in battlefield wounds, anastomosis hemorrhage and percutaneous intervention. Thus, there is a need for the development of novel bioactive materials to reduce the likelihood of hemorrhagic shock stemming from internal wounds. Here, we introduce an injectable hemostat from kappa-carrageenan and two-dimensional (2D) nanosilicates. Nanosilicates mechanically reinforce the hydrogels, provide enhanced physiological stability and accelerate the clotting time by two-fold. The sustained release of entrapped therapeutics due to presence of nanosilicates promotes enhanced wound healing. The multifunctional nanocomposite hydrogels could be used as an injectable hemostat for penetrating injury and percutaneous intervention during surgery.

1. Introduction

A penetrating injury from shrapnel is a serious obstacle in overcoming battlefield wounds and mortality [1]. Similarly, in anastomosis hemorrhage [2] and percutaneous intervention [3] during surgical procedures, localized hemostasis is essential. Given the high mortality rates due to hemorrhage, there is an unmet need to quickly self-administer materials that prevent fatality due to excessive blood loss. While progress has been made in the development of hemostats over the last decade, the performance of existing materials in healing internal wounds is not satisfactory. For example, commercially available hemostats, sealants and tissue adhesives such as QuikClot™ Floseal®, VITAGEL™, RDH bandage, Quick-Stat™ can be used to achieve hemostasis for external wounds [4]. These technologies can be used for surface/external wounds and require pressure to promote clotting which can be

* Corresponding author at: Department of Biomedical Engineering, Texas A&M University, College Station, TX 77843, United States.
E-mail address: gaharwar@tamu.edu (A.K. Gaharwar).

https://doi.org/10.1016/j.actbio.2018.01.045
1742-7061/

detrimental for high-risk situations such as internal wounds [5]. Many of these commercial hemostats have limitations such as need for pre-processing, batch variability and lack of shear-thinning characteristics [4,6]. Additionally, none of the current commercial hemostats are biofunctional. Thus, there is a need for the development of bioactive materials to reduce the likelihood of hemorrhagic shock stemming from internal wounds and subsequently stimulate tissue regeneration *via* release of bioactive factors.

Injectable hydrogels are promising materials for achieving hemostasis in case of internal injuries and bleeding, as these biomaterials can be introduced into a wound site using minimally invasive approaches [7,8]. Non-Newtonian characteristics of shear-thinning hydrogels result in a decrease in viscosity when subjected to shear strain [9]. An ideal injectable bandage should solidify after injection in the wound area and promote the natural clotting cascade. In addition, the injectable bandage should initiate a wound healing response after achieving hemostasis.

An emerging approach to integrate multi-functionality within hydrogel networks is to incorporate bioactive nanoparticles [10–15]. A range of synthetic nanoparticles have been incorporated within polymeric network to develop bioactive hydrogels [16,17]. Two-dimensional (2D) nanomaterials are a recent class of materials with unique structural and surface characteristics [18]. These nanoengineered ultrathin materials, with sheet or disc-like morphology, may generate therapeutic advances in the field of regenerative medicine and biomolecule delivery.

2D synthetic clays such as nanosilicates ($Na^{+}_{0.7}[(Mg_{5.5}Li_{0.3}Si_8O_{20}(OH)_4)]^{-}_{0.7}$, Laponite® XLG) have disc-shaped morphology and exhibit a dual charged surface [19,20]. Nanosilicates dissociate into nontoxic products (Na^{+}, Mg^{2+}, $Si(OH)_4$, Li^{+}) in physiological conditions and show cytotoxicity only at ten-fold higher concentrations ($LD_{50} \sim 4$ mg/mL) [21,22] compared to other 2D nanomaterials such as graphene ($LD_{50} \sim 100$ μg/mL) [23]. 2D nanosilicates can interact with a range of natural and synthetic polymers due to high structural anisotropy and charged surfaces [14,18,24,25]. Specifically, the presence of both cationic and anionic charges on the surface of the nanoparticle result in strong electrostatic interactions between nanosilicates and polymers [19,26,27]. These physical interactions generate the formation of transient netpoints within the matrix, which dissociate when subjected to high shear rates, resulting in shear-thinning characteristics [19,28–30]. These properties of nanosilicate-based hydrogels are investigated for a range of biomedical applications including minimally invasive approaches using injectable hydrogels, tissue engineering, drug and therapeutic delivery, and bioprinting [17,31–37].

We have recently demonstrated that the addition of nanosilicates also improves the injectability, physiological stability, and *in vivo* hemostatic performance [34]. The *in vivo* efficacy of these injectable hydrogels was observed as all the animals survived 4 weeks without secondary hemorrhage following initial injury. However, the drawbacks of this nanocomposite system were limited mechanical stiffness and lack of bioactive characteristics. To overcome these limitations, we propose to engineer injectable and mechanically resilient nanocomposite hydrogels consisting of bioactive nanosilicates and natural polysaccharide, carrageenan (CA). CA is a linear water-soluble sulfated polysaccharide polymer consisting of alternating β-(1,3)- and α-(1,4)-linked galactose residues and structure resembling to natural glycosaminoglycans (GAGs) [38–40]. Kappa carrageenan (κCA) contains one sulfate group per disaccharide and can be used to form ionotropic and thermotropic gels [39–41]. At low temperature, κCA undergoes sol-to-gel transition resulting from coil-helix transition of polymer chains. Additionally, in the presence of monovalent cations, mechanically stiff gels are produced due to strong ionic interactions between sulfate groups and ions.

Here we report the synthesis and fabrication of shear-thinning nanocomposites hydrogels made from κCA and nanosilicates. The addition of nanosilicates to κCA results in mechanically reinforced hydrogels networks with enhanced physiological stability. Nanosilicate addition also results in accelerated blood clotting by two-fold. The sustained release of entrapped therapeutics due to the presence of nanosilicates promotes enhanced *in vitro* wound healing. The multifunctional nanocomposite hydrogels could be used as an injectable hemostat for penetrating injury and percutaneous intervention during surgery.

2. Materials and methods

2.1. Materials and instruments

κCA was obtained from TCI Chemicals USA, Inc. and nanosilicates were obtained from Southern Clay Products Inc. (Laponite® XLG). The nanocomposites were crosslinked in potassium chloride (KCl) obtained from BDH Chemicals (VWR International, Houston, TX). Fourier-transform infrared spectroscopy (FTIR) peaks were investigated using FTIR spectrophotometer (Bruker vector-22, PIKE technologies, USA). Uniaxial compressive stiffness of the nanocomposite hydrogels was computed using ADMET Mtest Quattro Universal Testing System (ADMET, Massachusetts, USA). Nanodrop 3300 (Thermo Fisher Scientific Inc., USA) was employed to analyze the sustained release of fluorescein isothiocyanate labelled bovine serum albumin (FITC-BSA), purchased from Sigma-Aldrich, from the hydrogels. Scanning Electron Microscopy (SEM) (FEI Quanta 600 FE-SEM, USA fitted with Oxford Energy-dispersive X-ray spectroscopy system) was used to study the surface morphology of the nanocomposites. Blood component quantification was done using BD Accuri™ C6 Flow Cytometer (BD Biosciences, San Jose, CA, USA). For *in vitro* wound healing scratch assay, human umbilical vein endothelial cells (HUVEC, Lonza, USA) were used with vascular endothelial growth factor (VEGF, Life technologies, USA). Bovine citrated blood, obtained from the College of Veterinary Medicine, Texas A&M University, TX, USA, along with calcium chloride (BDH chemicals), sodium dodecyl-sulphate (VWR), Glutaraldehyde (VWR), Hexamethyldisilazane (HMDS) (Thermo Fisher Scientific), Micro BCA assay kit (Thermo Fisher Scientific) and Hemochron® 801 whole blood clotting system were used for hemostatic and quantification studies. Cell imaging was done by phase contrast microscopy using EVOS XL Core microscope (Electron Microscopy Sciences, PA, USA) and Zeiss Axio Vert.A1 microscope (Carl Zeiss, Oberkochen, Germany) for fluorescence imaging.

2.2. Synthesis of κCA-nanosilicates (Si) nanocomposites

Injectable precursors were obtained by combining different amounts of κCA (1 wt%) and nanosilicates (0, 0.5, 1 1.5, and 2 wt%) in deionized (DI) water. Both κCA and nanosilicates were dissolved separately and then mixed together to obtain a uniform dispersion. Uniformly mixed κCA-nanosilicate prepolymer solution (150 μl) was injected in circular poly(dimethylsiloxane) (PDMS) molds (3 mm high × 8 mm diameter). Subsequently, the PDMS molds containing prepolymer solution were incubated in 5 ml of 0.5 M KCl for 5 mins at room temperature to obtain ionically crosslinked nanocomposites. The ionically crosslinked nanocomposites were used to evaluate the physical, chemical and biological characteristics.

2.3. Physicochemical characterization

The shear thinning characteristics of prepolymer solutions (uncrosslinked) of 1% κCA, 1% κCA-1% nanosilicate and 1% κCA-2% nanosilicate was evaluated using shear rheology. Specifically,

viscosity of prepolymer solution was determined at varying shear rates (0.1–100 1/s). Shear-recovery of prepolymer solutions (uncrosslinked) was determined by subjecting to low (1%) and high (100%) strain and monitoring storage (G') and loss (G'') modulus. After ionically crosslinking the pre-polymer solution using KCl solution, mechanical properties were determined using uniaxial mechanical testing. κCA-nanosilicate hydrogels were used for mechanical studies using ADMET Mtest Quattro Universal Testing System (ADMET, Massachusetts, USA). One set with n = 5, was used immediately after preparation while the second (n = 5) and third (n = 5) sets were soaked in a 1X phosphate-buffered saline (PBS) solution for 12 h at 25 °C and 37 °C, respectively. 1 kN load cells were used to compute the load on the nanocomposite hydrogels against the positional movement of the load cells. Stress vs. Strain curves were plotted for each nanocomposite and compression moduli were calculated from the linear elastic region (0.05–0.15 strain) of stress-strain curve. FTIR-ATR spectroscopy was performed for different nanocomposite combinations, alongside κCA and nanosilicates individually, to analyze the interactions between κCA and nanosilicates. Surface topography of the nanocomposites was studied using SEM wherein samples were freeze dried and sputter coated with gold. Imaging was performed on the surface and longitudinal sections of the freeze-dried nanocomposites. Equilibrium water content (EWC) was determined by swelling the crosslinked hydrogels in 1X PBS for 1 h at 37 °C. After 1 h, the gels were removed and the wet weight (W_w) of the swollen gels was determined. The gels were then to obtain dry weight (W_d), and then EWC (%) = $(W_w - W_d) \times 100/W_w$ was calculated.

2.4. Physiological stability

Degradation of hydrogels (n = 5) was determined by analyzing weight loss in de-ionized water, 1X PBS and cell culture media. κCA and κCA-nanosilicate samples were prepared in batches of three. Each hydrogel (n = 3) was weighed (W_i) prior to incubation. The first batch was incubated in de-ionized water, the second in 1X PBS and the third in cell culture media at 37 °C. These hydrogels were weighed (W_t) at 6, 12, 24, 48 and 72 h of incubation. Images of the degradation of gels were captured in every solvent over a 72-h period. Weight loss (%) = $(W_i - W_t) * 100/W_i$ was calculated.

2.5. Cell adhesion, spreading and proliferation

Human mesenchymal stem cells (hMSCs) were cultured in normal growth media (AMEM, Hyclone), supplemented with 16.5% FBS (Atlanta Biologicals) and 1% penicillin/streptomycin (100 U/100 μg/mL; Life Technologies, USA) at 37 °C with 5% CO_2. Cells were trypsinized, neutralized with normal media, and then seeded at 10,000 cells/gel (~2 cm^2 gel surface) in normal media conditions. Cell morphology was evaluated by staining actin filaments according to manufacturer's protocol. Briefly, Phalloidin-iFluor 488 (Abcam) was utilized following fixation at Day 1 and Day 7 in a 2% glutaraldehyde solution (Sigma Aldrich) at room temperature for 20 min, treatment of 0.1% Triton-X100 for 5 min, and multiple PBS washes following each reagent. Cells were imaged using confocal microscopy (Leica TCS SP5). Cell area was measured from images using the program ImageJ. Alamar Blue (Thermo Fisher Scientific) was used to evaluate metabolic acidity of seeded cells to estimate cell proliferation, according to the manufacturer's protocol.

2.6. Hemostatic evaluation

Nanocomposite samples with varying concentration of nanosilicates (0%, 0.5%, 1%, 1.5%, 2%) and 1% κCA were prepared. These samples (n = 3) were then punched out using a 6 mm biopsy punch and placed in a 96-well plate. The samples were incubated in coagulation-activated blood (70 μl of 0.1 M calcium chloride ($CaCl_2$) + 100 μl of bovine blood containing sodium citrate) at 37 °C for pre-defined time. After 9 min, the aliquot of un-coagulated solution was removed and the well was washed twice with 1X PBS. The gel was removed from the well with the adhered blood clot. The gel was then imaged under a stereo microscope and photographed. The process was then repeated for 1, 2, 3 min all the way till 9 min. Then the first reading for initiation of clotting for every concentration was found and coagulation was analyzed for every 15 s between the two readings to increase accuracy. Quantitative analysis of the clotting time was performed using Hemochron® 801. 1% κCA and 1% κCA-2% nanosilicate hydrogels were placed in test-tubes containing Celite. 1 ml of Blood with 700 μl 0.1 M $CaCl_2$ was added to the test-tubes and coagulation time was obtained from the Hemochron® 801 Stress-controlled rheometer (Discovery Hybrid Rheometer (DH-2), TA instruments) was used to monitor blood clotting on hydrogel surface. First a thin layer of hydrogel (~100 μm) was prepared at the base geometry and subsequently a drop of blood (either citrated blood or coagulation-activated blood) was put on top of hydrogel surface. A time sweep experiment was performed to determine the increase in mechanical modulus correlating with the blood coagulation. For quantification of protein adsorption, the nanocomposite samples (n = 5) were incubated in whole blood at 37 °C for 2 min. The treated samples were then washed first with 1X PBS and then with 1X SDS solution to remove all adherent protein. This solution was used to obtain protein content for individual concentrations of the nanocomposites as per the protocol provided in the MicroBCA assay kit. For blood component quantification, κCA-nanosilicate samples of larger dimensions (22 mm diameter, 3 mm thickness) were created. These samples were placed in 50 ml Falcon tubes containing citrated bovine whole blood as well as plasma poor blood and were allowed to stand for 2 min. The nanocomposite hydrogels were then removed and washed with 1X PBS. The PBS solution was then run through the BD Accuri C6 Flow Cytometer and the quantity of blood components in individually treated samples was analyzed. Tissue culture polystyrene (TCPS) was used as a control. SEM imaging of platelets on the hydrogel surface was done by critical point drying the samples in HMDS after incubating in blood for 2 min and serial dehydration in alcohol followed by fixing of cells in 2.5% glutaraldehyde.

2.7. Protein release kinetics

0.15% (wt/v) stock solution of FITC-BSA was prepared for release profile studies. 500 μl of κCA-nanosilicate precursors of different concentrations, were added to 1 ml of the nanocomposite solutions individually to obtain final FITC-BSA concentration of 0.05% (wt/v). From this solution, 150 μl was taken in pre-formed PDMS molds and ionically crosslinked with 5% (wt/v) KCl solution to form hydrogels. These hydrogels were placed in a 24 well plate each containing 1 ml 1X PBS solution. The samples were maintained at 37 °C for 20 days and the release was monitored by reading the fluorescence of FITC-BSA at 520 nm in a Nanodrop 3000. The data obtained was quantified against the relative fluorescence unit (RFU) value of FITC-BSA using a standard curve to find release percentage at every interval. Release of FITC-BSA was also captured using a stereomicroscope with a green filter for both κCA as well as κCA-nanosilicate samples.

2.8. In vitro scratch-assay test

Nanocomposite samples entrapping VEGF to a final concentration of 50 ng/ml were prepared. Nanocomposites hydrogels were added to transwell inserts for 7 days to collect the released protein

in cell culture media. The cell culture media loaded with released protein was used to evaluate the activity of protein (VEGF). Human umbilical vein endothelial cells (HUVECs) were cultured in a 24-well plate and allowed to reach a density of 10^4 cells per well. Subsequently, the cells were starved for 12 h. After starvation, a scratch was made on the surface of the cell monolayer using a p200 pipette tip to mimic the conditions of a scratch wound. Thereafter, cell culture media was replaced by media containing released protein. The cell layer was observed and imaged at intervals of 0, 12, 24 and 36 h using phase contrast microscopy in EVOS XL Core.

2.9. Migration assay

Nanocomposite hydrogels (1% κCA/2% Si) entrapping VEGF at 50 ng/ml final concentration were placed in a 24 well plate. A transwell containing 10^4 cells on its top layer was placed inside the well containing the nanocomposite hydrogel so that the gel surface was not touching the transwell. The cells were allowed to migrate for 1 day towards the lower layer of the transwell and then dried and fixed using 2.5% glutaraldehyde. The fixed cells were stained using DAPI and Phalloidin iFluor 488 (Abcam) dyes as per manufacturer's protocol. Migration was observed on the lower layer of the transwell using fluorescence microscopy. The results were compared with migration in presence of nanocomposite sample without VEGF and 1% κCA hydrogel. Media with and without VEGF served as controls.

2.10. Statistical analysis

The data are presented as mean ± standard deviation (n = 3–5). One-way analysis of variance (ANOVA) with Tukey's post hoc test for pairwise comparison was performed to obtained statistical difference between samples. Statistical significance designated with $^*p < 0.05$, $^{**}p < 0.01$, and $^{***}p < 0.001$.

3. Results and discussion

3.1. Injectable, shear-thinning and self-recovery pre-crosslinked nanocomposites

Pre-polymer (uncrosslinked) compositions from κCA and nanosilicates were obtained by combining different ratio of κCA and nanosilicates (Fig. 1a). With the increase in κCA and/or nanosilicate concentration, an increase in viscosity was observed. We also observe that the addition of nanosilicates to κCA results in shear-thinning characteristics. The flow characteristics of pre-polymer solutions were quantified using shear rheology. We determined the viscosity of pre-polymer solutions with respect to increasing shear rates at physiological temperature (37 °C).

A thixotropic material will enable the injection of pre-polymer solution using minimal force with very low viscosity following extrusion. The pre-polymer solution of κCA (1 wt%) showed liquid-like behavior at 37 °C as viscosity was <1 P at different shear rates (0.1–100 1/s). The addition of nanosilicates (1 and 2 wt%) to κCA (1 wt%) provided a significant increase in pre-polymer viscosity between 10 and 100 P across varying shear rates (0.1–100 1/s), showing shear-thinning behavior (Fig. 1b). In addition, incorporation of nanosilicates to κCA (1 wt%) also results in enhanced shear-recovery ability of pre-polymer solution (Fig. 1c). Pure κCA (1 wt%) solution had minimum shear-recovery due to low viscosity of solution. At low strain (1%), κCA has a storage modulus (G′) of ~3 Pa. The addition of 1% and 2% nanosilicates increased the storage modulus to ~90 and ~350 Pa, respectively. When subjected to high strain (100%), κCA demonstrated network breakdown as evident from reduced storage modulus (<1 Pa) with no recovery

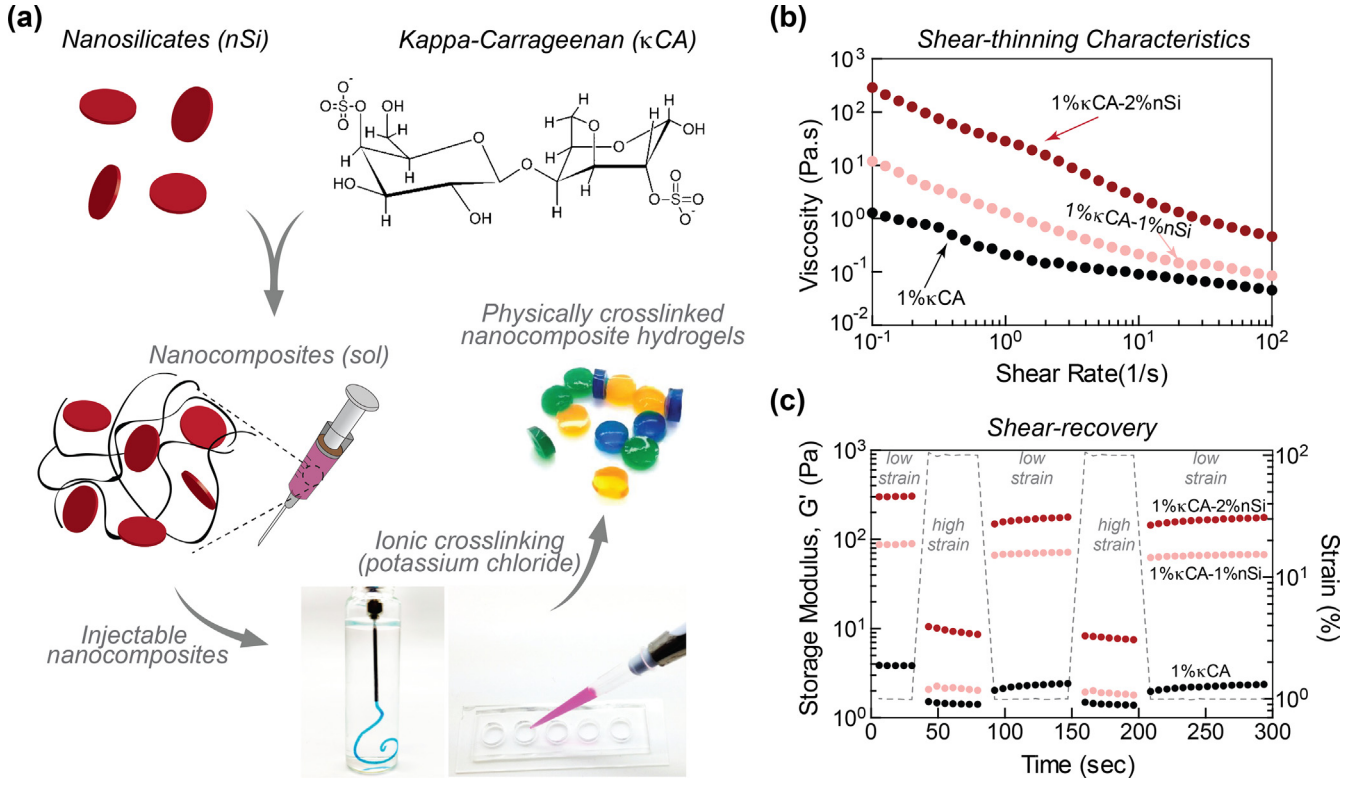

Fig. 1. Synthesis of κCA-nanosilicate hydrogels. (a) Schematic representation of the fabrication of injectable nanocomposite hydrogels by combining kappa carrageenan (κCA) and nanosilicates (Si) crosslinked in KCl solution. (b) The shear-thinning characteristics of pre-polymer hydrogels indicate that the addition of nanosilicates increases viscosity at different shear rates. (c) The addition of nanosilicates impart self-recovery characteristics, as storage modulus (G′) of pre-polymer solutions show more than 80% recovery after application of high strain. This indicates rapid recovery of nanocomposite gels after injection.

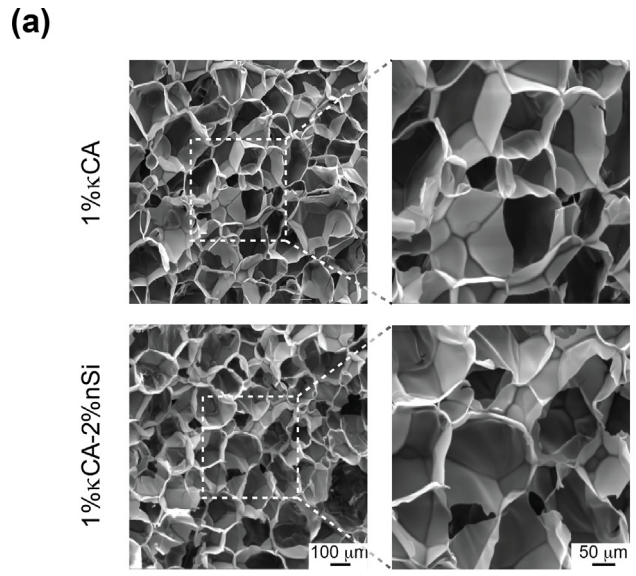

Fig. 2. Ionically crosslinked κCA-nanosilicate hydrogels. (a) The addition of nanosilicates does not affect interconnected and porous microstructure. (b) FTIR spectra for nanocomposites indicate presence of nanosilicates as shown by characteristic peak for Si—O—Si bond stretching at 1068 cm^{-1}.

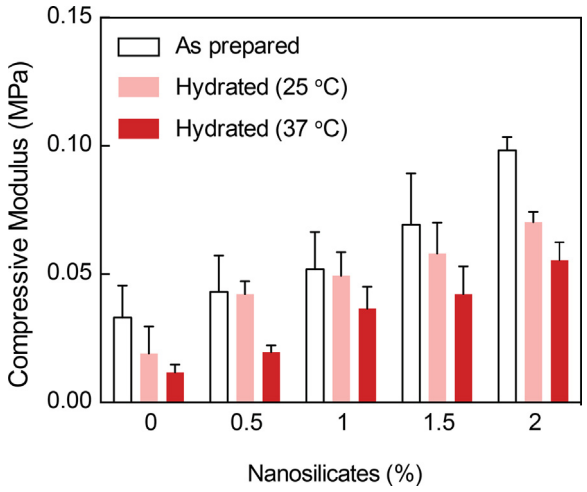

Fig. 3. Nanosilicates reinforce the mechanical properties of κCA hydrogels. A linear increase in mechanical stiffness was observed due to increase in nanosilicates (0.5, 1, 1.5, and 2%). Compressive moduli of as-prepared, and hydrated nanocomposites also show similar characteristics.

after being subjected to low strain. The addition of nanosilicates imparted mechanical recovery characteristics to the κCA hydrogels as observed from the recovered storage modulus (~80%). Both shear-thinning with mechanical stability and mechanical-recovery characteristics of nanocomposites that were obtained after the addition of nanosilicates indicated the potential suitability of the nanocomposite for rapid localized delivery in a clinical or emergency setting.

3.2. Ionically crosslinked nanocomposites

After uniformly mixing a pre-polymer solution of κCA and nanosilicates, the composition was subjected to 0.5 M KCl to obtain physically crosslinked nanocomposites. The pre-polymer solution forms a strong hydrogel quickly (<2 mins) upon KCl treatment. The gelation occurs due to formation of hydrogen bonds and ionic interactions, as κCA undergo coil-helix conformational transition, rendering ionotropic and thermotropic hydrogels. We used these physically crosslinked hydrogels to investigate the effect of nanosilicate addition to κCA on physical, chemical and biological characteristics.

The effect of nanosilicates on κCA microstructure was investigated using electron microscopy (Fig. 2a). Lyophilized samples of both κCA and κCA-nanosilicate hydrogels showed highly interconnected and porous networks; there was no significant effect on pore size following nanosilicate addition, indicating nanosilicate additions do not alter the micro-architecture of the hydrogel network. The presence of nanosilicates within crosslinked nanocomposites was investigated using Fourier-Transform infrared spectroscopy (FTIR) (Fig. 2b). In κCA, a strong peak observed at 1079 cm^{-1} was assigned to O═S═O symmetric bond (stretching). Additionally, the sharp peaks at 925, 847 and 1260 cm^{-1} were associated with asymmetrical C—O vibration of 3,6-anhydro-D-galactose, the pseudo-symmetrical C—O—S vibration of a sulfated group of β-1,3-linked residue, and antisymmetric stretching O═S═O vibration, respectively. The smaller peak at 1644 cm^{-1} was correlated with C═O stretching of an amide. The inclusion of nanosilicates in nanocomposite hydrogels was confirmed by the presence of a sharp peak at 1068 cm^{-1} corresponding to Si—O—Si stretching. Nanocomposite samples showed a reduction in the intensity of the peaks at 1644, 1260, 925 and 847 cm^{-1}, when compared with κCA. In addition, the 1079 cm^{-1} peak of κCA was shifted below 1000 cm^{-1} for nanocomposites, indicating physical interactions between O═S═O symmetric bond stretching and Si—O—Si.

3.3. Nanosilicates enhance mechanical stiffness

The high surface area and charged nature of nanosilicates were expected to reinforce κCA hydrogels. We investigated the effect of nanosilicate addition to κCA hydrogel on mechanical stiffness using uniaxial compression testing (Fig. 3). Nanocomposite hydrogels with 1 wt% κCA were reinforced with 0, 0.5, 1 and 1.5 wt% nanosilicates. The increase in nanosilicates concentrations resulted in an increase in compressive modulus for crosslinked hydrogels. This indicated that nanosilicates reinforced the κCA network. The presence of negative and positive charges on the surface of nanosilicates could have enhanced electrostatic interactions with κCA, which contains charged side groups capable of interacting with

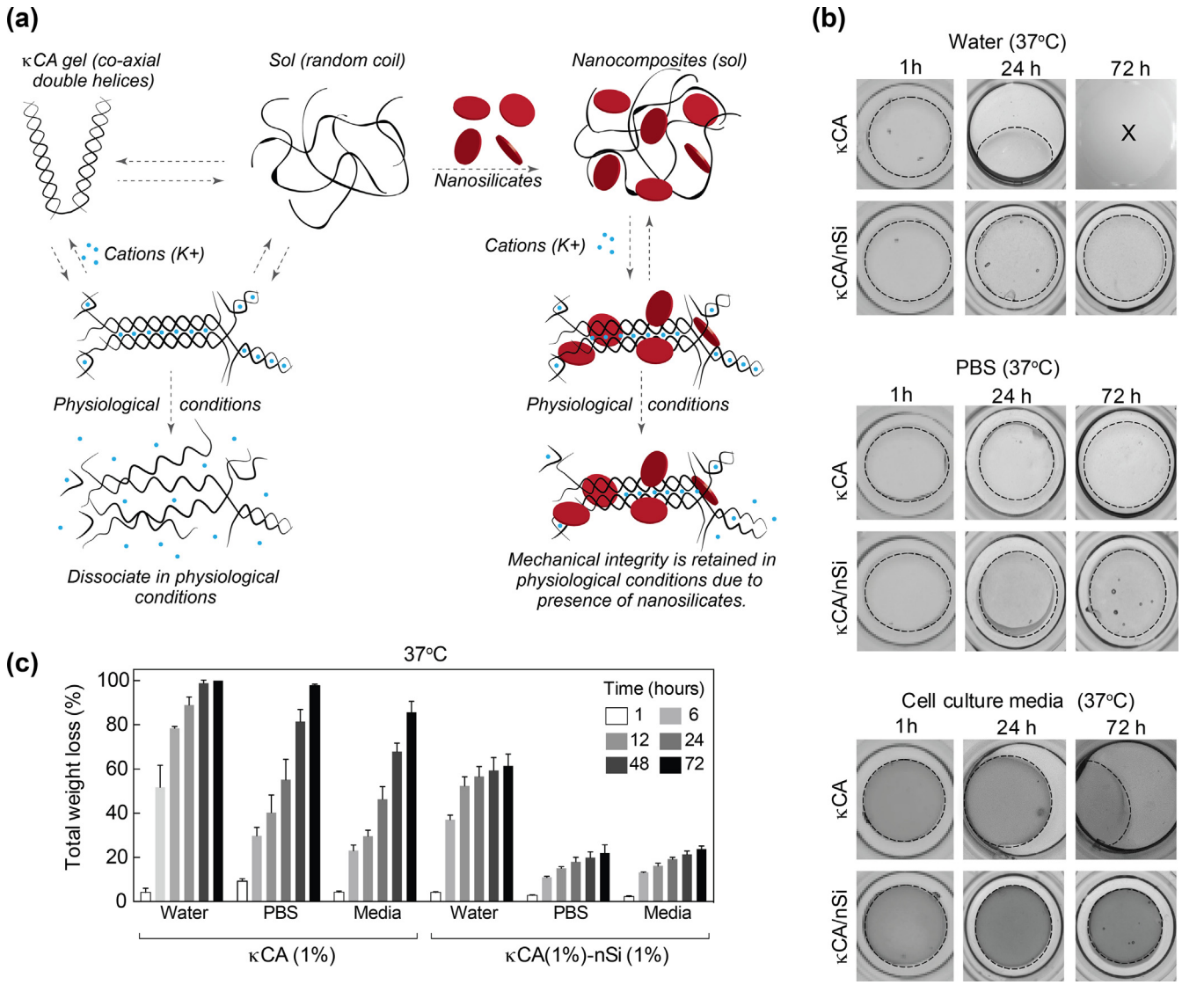

Fig. 4. Nanosilicates improve physiological stability of nanocomposite hydrogels. (a) The addition of nanosilicates provide stability to ionically crosslinked κCA network by acting as a physical crosslinker and/or retaining ions. In physiological conditions, the κCA chains fail to hold on to the K^+ cations obtained during crosslinking. But in presence of nanosilicates, these cations tend to remain attached to the κCA chains thus improving mechanical strength. (b) Microscope images showing degradation of the κCA samples in deionized water, PBS and cell culture media at physiological temperature (37 °C). The κCA-nanosilicate hydrogel samples retain their shape and size up to 72 h in all three solvents with minimal weight loss. (c) Total weight loss of κCA and κCA-nanosilicate in water, PBS and media over a period of 72 h. κCA samples show exponential weight loss in all solvents whereas κCA-nanosilicate hydrogels show minimal weight loss.

nanosilicates under physiological pH conditions. The mechanical stiffness of nanocomposites was compared amongst three different conditions, including as prepared, and hydrated in PBS at 25 °C and 37 °C. The overall trend indicated that the as prepared samples showed higher mechanical stiffness compared to the hydrated samples. The nanocomposites hydrated at 37 °C showed lower mechanical stiffness compared to the nanocomposites that hydrated at 25 °C. The decrease in mechanical properties after hydration at higher temperature may be due to leaching out of uncrosslinked κCA (sol content) and/or increased chain mobility associated with the higher water content or temperature.

3.4. Nanosilicates enhance physiological stability

Water holding capacity of a hydrogel gives an insight into the stability of the hydrogel when subjected to physiological conditions. Thus, equilibrium water content was determined after soaking the crosslinked gels in PBS at 37 °C for 1 h. The results show that addition of nanosilicates reduces equilibrium water content of hydrogels, i.e. 1% κCA (90.2 ± 1.1%) and 1% κCA-1% nanosilicate (97.1 ± 0.5%). The physiological stability of κCA and nanocomposite hydrogels was determined by subjecting the hydrogels to a variety of aqueous environments – deionized water, PBS, and media, all at 37 °C. Nanosilicates are expected to sequester K^+ ions, which play a crucial role in κCA crosslinking and physiological stability (Fig. 4a). In deionized water, κCA showed significant weight loss during initial 6 h and was completely degraded within 72 h (Fig. 4b and c). This corroborates with an earlier study which reported that ionic crosslinking of κCA was unstable in deionized water due to ion release from the gel, subsequently accelerating dissolution of hydrogels [42]. A similar trend was observed for κCA hydrogels in the other environments with virtually complete degradation of the hydrogel within 72 h. The addition of nanosilicates (1%) significantly improved the physiological stability of the nanocomposite hydrogels by extending longevity of the constructs. It is noteworthy that nanocomposites in PBS and media displayed

<20% weight loss after 72 h, highlighting its ability to retain a local concentration of K^+ ions. The enhanced structural stability of nanocomposites under physiological conditions indicated strong ionic interactions between nanosilicates and κCA. Additionally, we investigated the interaction between nanosilicates and potassium ions by determining the electronegativity of nanosilicates in de-ionized water and in aqueous 0.5 M KCl solution. A significant shift in zeta potential towards positive values was observed in the KCl solution (−5 mV) compared to deionized water (−34.5 mV). This corroborated our hypothesis that nanosilicates sequester K^+ ions on the surface thereby increasing zeta potential.

Earlier studies also support the ability of nanosilicates to physically reinforce a hydrogel network [31,34,43]. For example, the addition of nanosilicates to gelatin or poly(ethylene glycol) (PEG) hydrogels resulted in significantly enhanced compressive modulus [31,34,43]. Such increase in mechanical characteristics are attributed to enhanced physical interactions between polymeric backbone with charged nanosilicate surfaces that results in formation of reversible "loops" and "chain" [15,18]. Although the exact interactions between polymeric chains and the nanosilicate surface is not known, they may be attributed to hydrogen bonding, ionic interactions, and electrostatic interactions as the surfaces of nanosilicates are dual charged (i.e. edge is positively charged, while the faces are negatively charged) [19,20]. It can be speculated that negatively charged sulfate groups of κCA might interact with positively charged edge of nanosilicates *via* electrostatic interactions. The presence of ions, such as K^+, can further facilitate the interaction between negatively charged nanosilicate surface with sulfate groups of κCA. Overall, our current study supports the ability of nanosilicates to physically reinforce a polymeric hydrogel network.

In addition, the increase in mechanical stiffness will also help in physically obstructing the flow of blood and achieve rapid hemostasis compared to previously reported gelatin-nanosilicate hydrogels [34]. As prepared 1% κCA-2% nanosilicate hydrogels have compressive modulus of 197.6 ± 19.5 kPa, and then subsequently reduce to 84.5 ± 18.5 kPa in hydrated conditions at 37 °C. The maximum mechanical stiffness obtained using gelatin-nanosilicate system was ~1–10 kPa [34]; it would be difficult to translate this system into clinical practice because the diastolic and systolic blood pressure in a healthy human are ~10.6 kPa (~80 Hg) and ~16 kPa (~120 mm Hg), respectively. Thus, κCA-nanosilicate hydrogels have potential to act as physical barrier to achieve hemostats.

3.5. Nanosilicates enhance cell adhesion and spreading

Biological interactions of nanocomposites with mammalian cells were investigated by seeding hMSCs on hydrogel surfaces. Due to lack of cell binding domains on κCA backbone, cells do not adhere to κCA (1%) hydrogels and show minimum adhesion and spreading (Fig. 5a and b). However, the addition of nanosilicates to κCA,

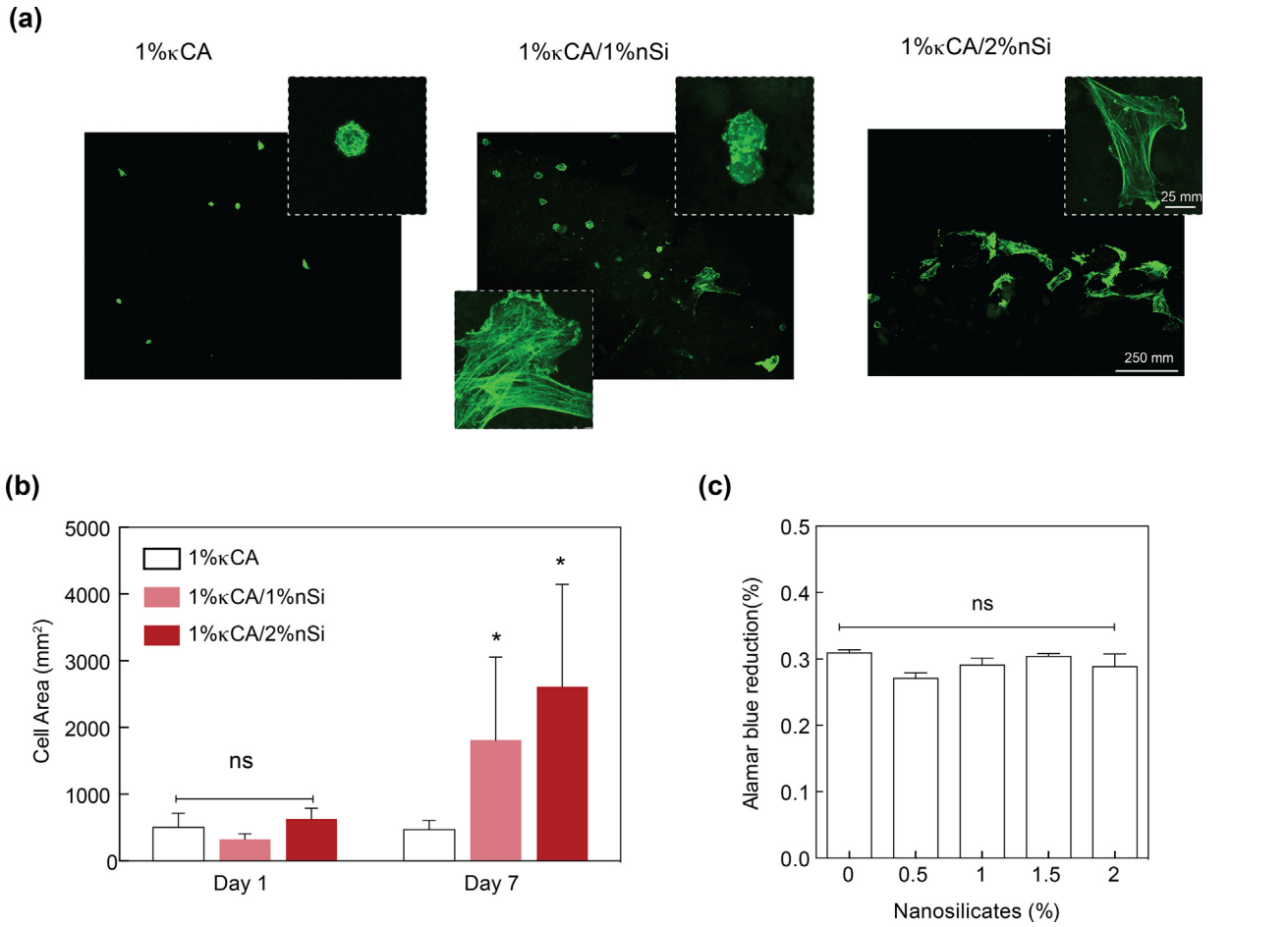

Fig. 5. Nanosilicates induce cell adhesion characteristics and support proliferation. (a) hMSCs readily attach and proliferate on κCA and κCA-nanosilicate hydrogels. (b) The addition of nanosilicates to κCA hydrogels showed enhanced cell spreading as indicated by increase in cell area. (c) The seeded cells readily proliferated on κCA and κCA-nanosilicate hydrogels as evident by metabolic activity determined using Alamar blue assay.

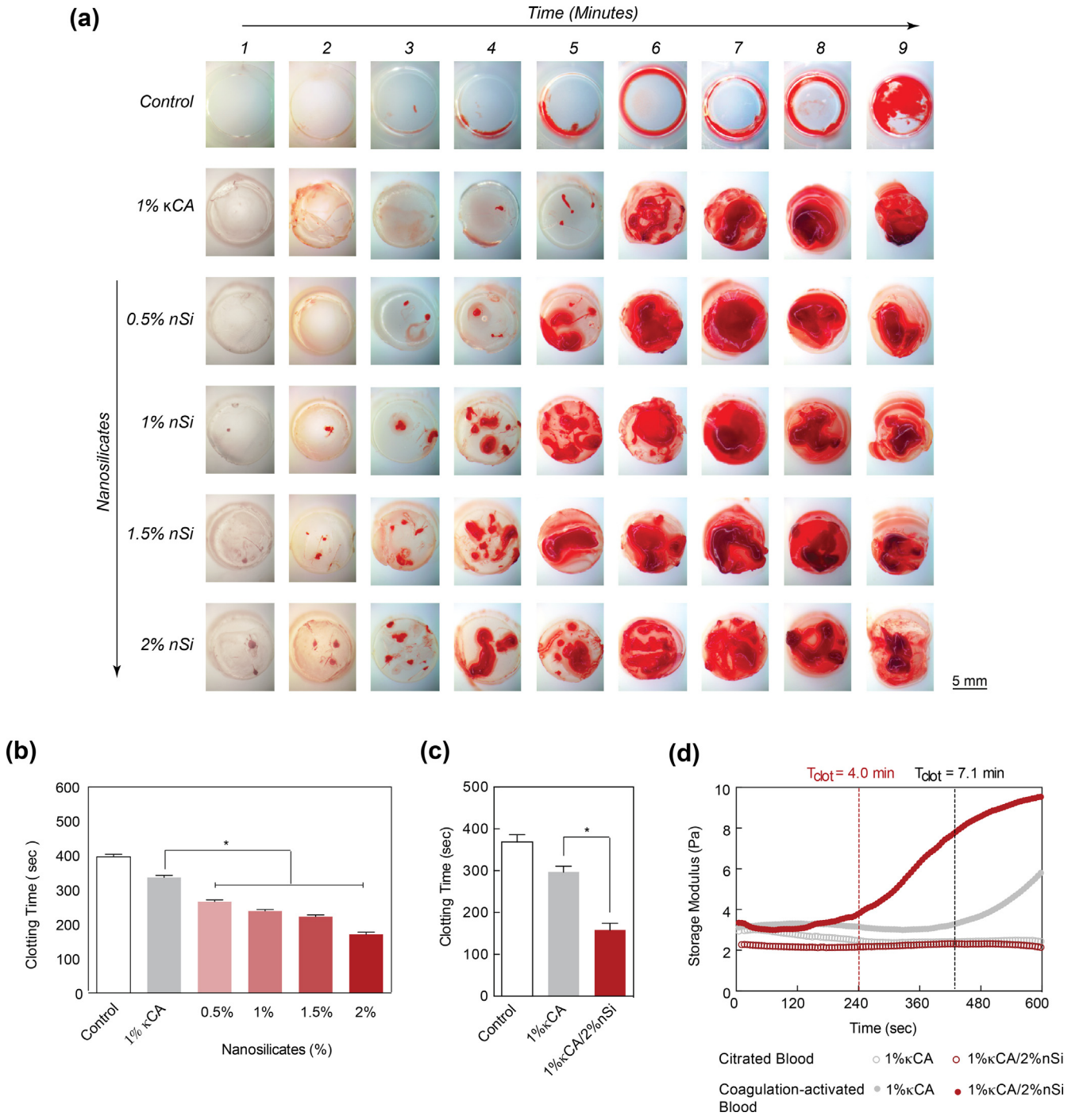

Fig. 6. Nanosilicates accelerate blood clotting necessary to attain hemostasis. (a) The images show clotting kinetics of whole blood with respect to time and nanosilicate concentration in κCA hydrogels. The control (TCPS) shows clotting between 8 and 9 mins, while κCA shows formation of clot ~6 mins. The addition of nanosilicates significantly decreases the clotting time. (b) A quantitative analysis of clotting time vs nanosilicate concentration shows a decrease in clotting time by more than two-fold. (c) Activated clotting time shows that addition of nanosilicate significantly decreases clotting time. (d) The clotting time on κCA and κCA/Si nanocomposite was also determined using time sweep experiment by monitoring storage modulus, support ability of nanosilicate to accelerate clotting.

resulted in enhanced cell adhesion and spreading. Following seven days of culture in normal media conditions, 1% κCA hydrogels containing 2% nanosilicate displayed spreading of cells over a significantly ($p < 0.01$) larger areas than that of pure κCA gels. Specifically, composite gels with 2% nanosilicate produced an average increase in area by 400%, while pure κCA gels did not show any increase in area after seven days of culture. Due to the inherent lack of binding moieties within the κCA backbone, cells maintain a round morphology on the surface of pure gels. Increasing the nanosilicate concentration, however, seemingly provided electrostatically-driven adhesion sites for proteins found within culture media, thereby, enabling cell membrane binding. Improvements in cell spreading may translate to augmented compatibility and regenerative responses when placed in *in vivo* environments. The effect of nanosilicates on cell proliferation was monitored using Alamar Blue proliferation assay (Fig. 5c). The assay demonstrated

no difference in cell metabolic activity following impregnation of the hydrogel matrix with nanosilicates indicating nanocomposite cytocompatibility.

3.6. Nanosilicates enhance platelet adhesion and induce blood clotting

The ability of nanocomposite hydrogels to achieve hemostasis was investigated by determining clotting time of blood in the presence of nanocomposites (Fig. 6a and b). The clotting time of bovine blood in TCPS was ~8 mins, similar to previously reported literature [44]. Due to their highly anionic nature, κCA (1%) hydrogels were able to reduce the blood clotting time to <6 mins. Our study indicates potential use of κCA for hemostasis, which is not reported in literature. The addition of 2% nanosilicates to 1% κCA, further reduced the clotting time to <3 mins, highlighting the ability of nanosilicates to enhance clotting. The amount of clot formed on nanocomposite hydrogels increased with greater nanosilicate concentrations. Compared to TCPS control, nanocomposite hydrogels with 0.5, 1, 1.5 and 2% nanosilicates, showed 33, 40, 44 and 57% decrease in clotting time, respectively, as opposed to a 16% decrease in κCA controls lacking nanosilicates. We further conducted a kaolin activated clotting time test on our nanocomposite hydrogels using the Hemochron™ 108 series. We obtained similar results on clotting time with 1% κCA/2% nanosilicates showing almost half the time taken compared to 1% κCA and a negative control with no hydrogel (Fig. 6c). These observations were subsequently confirmed using shear rheology (Fig. 6d). Specifically, we monitored the coagulation of citrated and coagulation-activated blood on 1% κCA and 1%κ CA/2% nanosilicate hydrogel surfaces. The results demonstrated nanocomposites (~4 mins) expedited the clotting process relative to a pure κCA hydrogels (~7 mins) due to the inclusion of nanosilicates.

To understand the potential mechanism behind enhanced blood clotting on the hydrogel surface loaded with nanosilicates, we quantified the blood-hydrogel interactions. Specifically, we quantified the amount of blood components (platelets and red blood cells (RBCs)) on hydrogel surface following nanosilicate introduction using flow cytometry (Fig. 7a). The addition of nanosilicates to κCA results in enhanced adhesion of RBCs and platelets, when hydrogels were subjected to whole blood or plasma poor blood. This indicate that the surface of hydrogels plays a major role in platelet activation and subsequent clotting.

To further evaluate the role of hydrogel surface, we determined the nanosilicate-κCA interactions and its effect on zeta potential. The decrease in blood clotting time can be attributed to the highly negative charge of the hydrogel surface. The zeta potential of κCA was found to be −49 ± 4.5 mV, and addition of 0.5, 1, 1.5 and 2% nanosilicates further reduces the zeta potential to −58.9 ± 0.8 m V, −58.7 ± 1.5 mV and −58.4 ± 3.1 mV and −60.2 ± 5.7 mV, respectively. Earlier reports highlighted that a negatively charged surface triggers intrinsic coagulation pathway by activating Hageman factor (FXII). It is also reported that a negatively charged surface activates platelets [45,46]. To investigate platelet activation, we soaked κCA and nanocomposite hydrogels in fresh blood for 2 mins and imaged the hydrogel surface. We observed minimal platelet adhesion on κCA hydrogels and no change in platelet morphology (Fig. 7b and c); however, the addition of nanosilicates to κCA resulted in a significant increase in platelet adhesion and activation, as indicated by number of platelets adhered on the hydrogel surface and transformation in platelet morphology, respectively. To quantify the protein adsorption, we incubated hydrogels in a fluorescein isothiocyanate-labeled bovine serum albumin (FITC-BSA) solution and determined the amount of adsorbed protein (Fig. 7d). Increasing the concentration of entrapped nanosilicates imparted a greater protein adhesion response; specifically, we

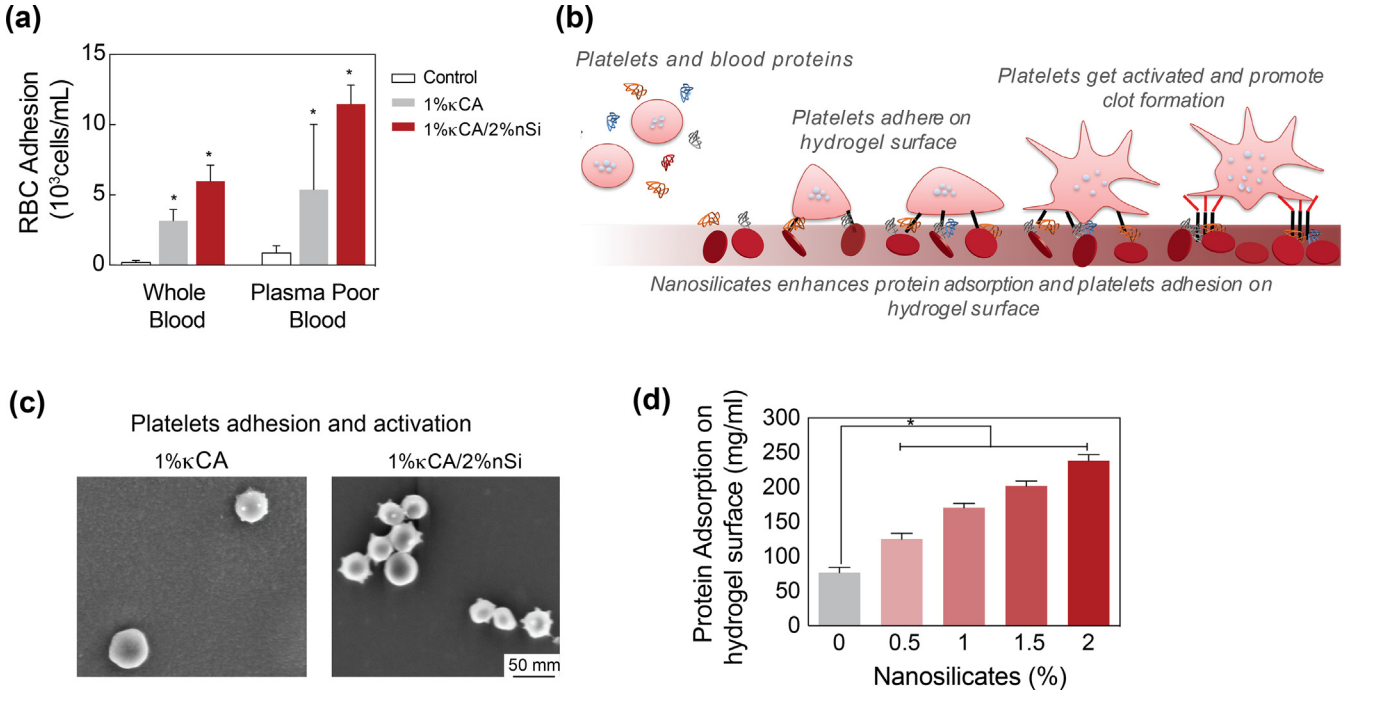

Fig. 7. Nanosilicates promote platelet adhesion to attain hemostasis. (a) The accelerated clotting on the nanocomposite might be attributed to enhanced adhesion of blood components including red blood cells (RBC) and platelets as determined by flow cytometry. (b) Schematic representation of the possible mechanism for interaction of nanosilicates with platelets leading to their adhesion to the nanocomposite surface and subsequent activation. (c) SEM images of hydrogel surface showing adhered platelets. κCA-nanosilicate hydrogels have enhanced adhesion of platelets in comparison to κCA. The presence of nanosilicates also activate platelets as shown by the change in platelet morphology. (d) The enhanced adhesion of RBCs and platelets is attributed to enhanced protein adhesion due to nanosilicate addition to κCA. (For interpretation of the references to colour in this figure legend, the reader is referred to the web version of this article.)

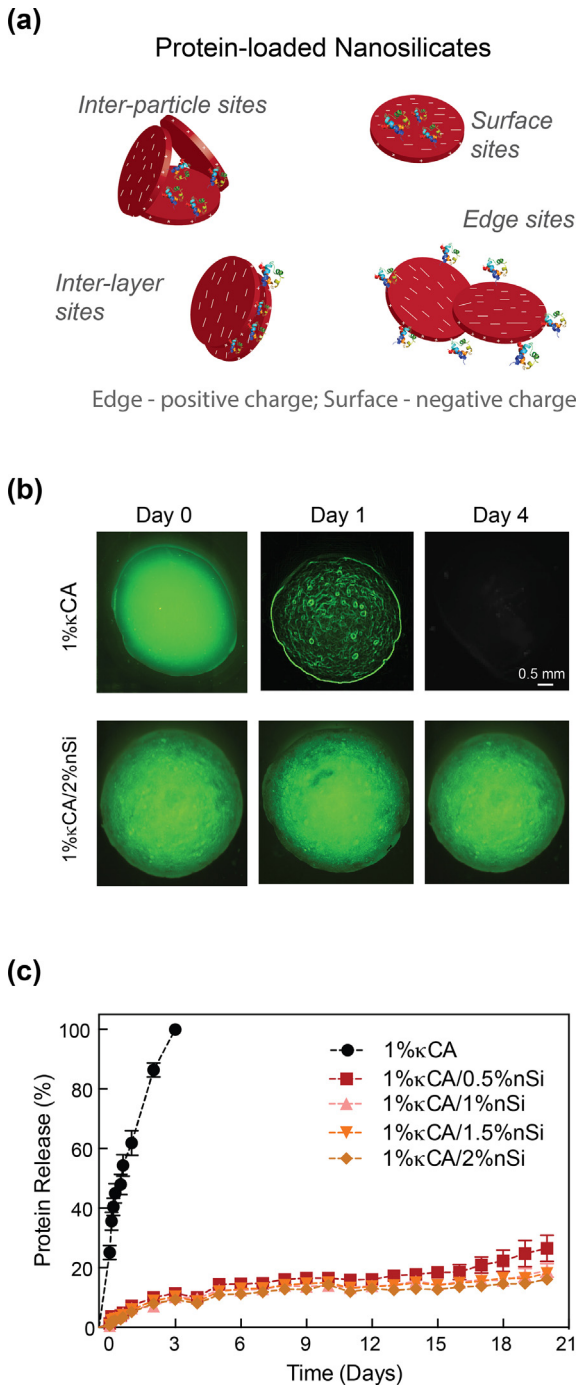

Fig. 8. Nanosilicates result in sustained release of protein from κCA-nanosilicate hydrogels. (a) Schematic representation of the possible mechanism of interaction between protein and nanosilicates which ensures sustained and controlled release. (b) Fluorescence images of FITC-BSA loaded κCA and κCA-nanosilicate hydrogel samples incubated in PBS at 37 °C over the course of 4 days. The absence of green fluorescence in κCA sample by day 4 is indicative of 100% release of FITC-BSA. (c) Graphical representation of the release profile of FITC-BSA being released from κCA and κCA-nanosilicate samples. A burst release of FITC-BSA from κCA samples is seen within day 1 and complete release within day 4. κCA-nanosilicate samples show controlled release (~40%) until day 21 irrespective of nanosilicate content. (d) The addition of a protein such as VEGF does not alter the clotting characteristics of nanocomposites. (For interpretation of the references to colour in this figure legend, the reader is referred to the web version of this article.)

observed almost a four-fold increase in adsorbed protein following the addition of 2% nanosilicates to κCA hydrogels. Therefore, the increase in blood component adhesion can be most likely attributed to the enhanced protein adhesion on the nanocomposite surface due to presence of nanosilicates.

3.7. Nanosilicates result in sustained release of therapeutics

Growth factors or soluble-secreted signaling polypeptides are capable of directing specific cellular responses under *in vitro* and *in vivo* conditions [47,48]. Sustained release of growth factors has been shown to enhance the therapeutic efficiency compared to bolus delivery [49]. Because most growth factors falter due to short half-lives and susceptibility to proteinases, supraphysiologic dosages of growth factor are required, which result in several negative side-effects due to unregulated signaling [50]. Therefore, sequestering growth factors within hydrogels can significantly enhance their bioactivity and efficacy to direct tissue regeneration [17,51]. Due to their unique 2D nanostructure and surface charge characteristics [18], nanosilicates are expected to physically conjugate biomolecules (Fig. 8a) and result in sustained release.

To investigate the effect of nanosilicates on sequestering therapeutics, we encapsulated FITC-BSA, as a model protein with κCA and nanosilicate nanocomposite hydrogels. The release of entrapped fluorescent protein was monitored in physiological conditions (PBS and 37 °C) using a spectrophotometer. κCA hydrogels showed initial burst release of encapsulated protein during the first 4–8 h and complete protein release in 72–96 h (Fig. 8b and c). From dissolution studies, κCA hydrogels disintegrated within ~72 h and subsequently the release of entrapped FITC-BSA directly correlated to the stability of κCA hydrogels. The addition of nanosilicates suppressed the burst release profile of entrapped protein and demonstrated sustained release of FITC-BSA over a period of 21 days. In the presence of 0.5% nanosilicates, the cumulative release of entrapped protein after 21 days was only ~40%. Considering that nanosilicates have a distinct structure that generates a positive charge along the edges and a permanent negative charge on the surface, we hypothesize that the unique charge arrangement and high surface-to-volume ratio enhance the ability of nanosilicates to physically interact with a range of proteins with a basic isoelectric point. The activity of these proteins can be maintained because nanosilicates physically adsorb the biomolecules on the surface without covalent crosslinking. In addition, the protein-protein electrostatic interactions dominate over nanoparticle-protein interactions when pH of the environment is maintained close to the isoelectric point of the proteins [52]. The inclusion of protein within nanocomposite hydrogels did not alter the clotting ability of nanocomposites. Consequently, the addition of higher amounts of nanosilicate did not significantly alter the release kinetics of entrapped protein. It is expected that the sustained release of sequestered therapeutics can reduce the effective therapeutic concentration utilized. Overall, sustained release of entrapped protein from the nanocomposites without burst release indicates the ability of κCA-nanosilicate hydrogels for therapeutic delivery targeting regenerative applications.

3.8. Nanocomposites result in sustained release of VEGF and enhanced wound healing

For accelerated wound healing, vascular endothelial growth factor (VEGF), a glycosylated protein homodimer, was found to be clinically effective [53,54]. VEGF facilitates cellular migration into the wound region and supports proliferation of endothelial cells for accelerated wound closure. VEGF is present during all stages of the wound healing cascade and it significantly stimulates multiple stages in the angiogenic cascade and re-epithelialization of damaged tissue. In acute and chronic wounds, levels of VEGF decrease due to proteolytic microenvironment and/or excessive blood loss [55]. External delivery of VEGF has enhanced wound

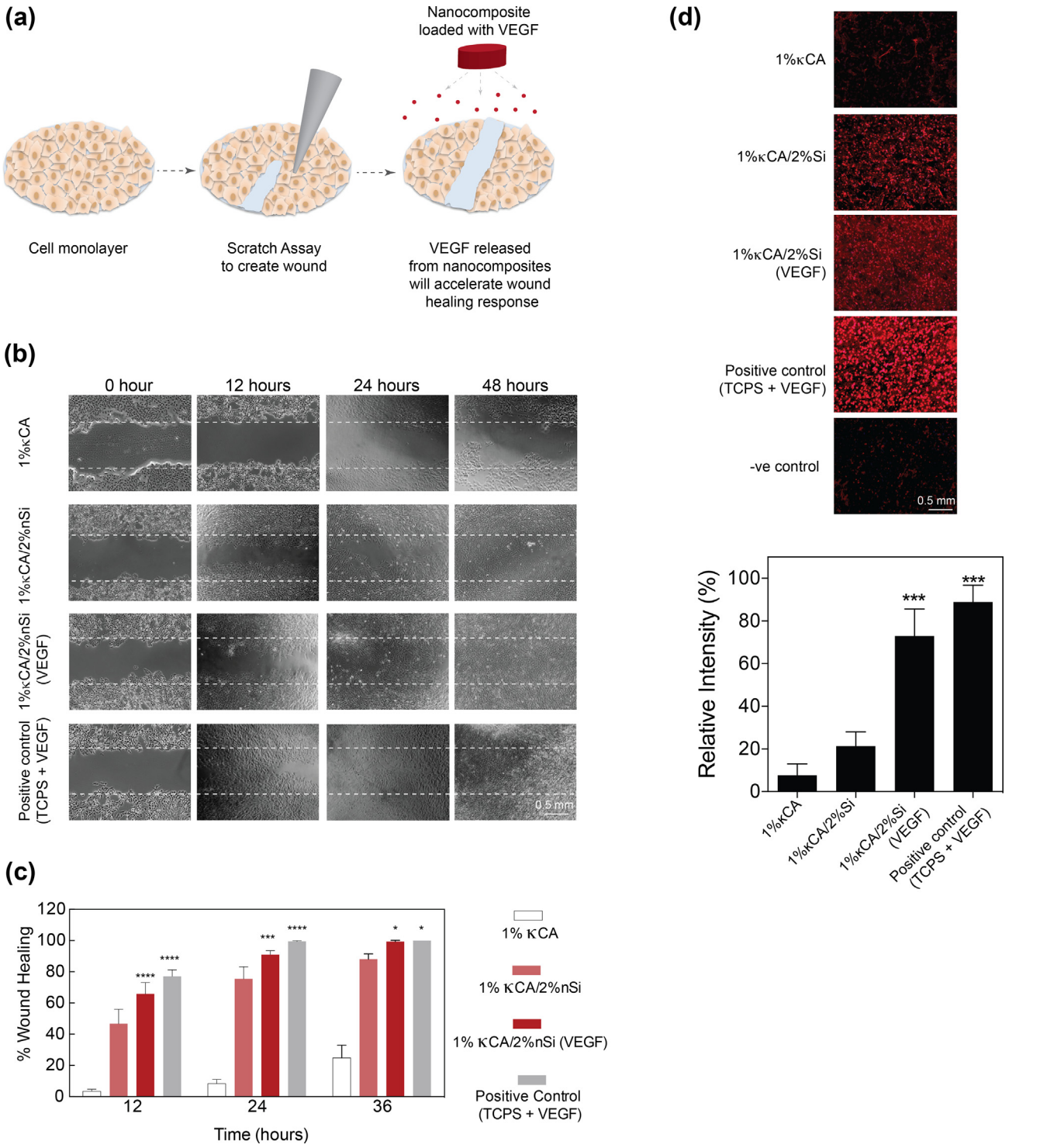

Fig. 9. Nanosilicates enhance VEGF release and promote wound healing. (a) Schematic representation of the scratch assay to test the wound healing potential of the κCA-nanosilicate hydrogels. VEGF released from the nanocomposite hydrogels promotes cell migration, thus promoting scratch wound healing. (b) Phase contrast images of human umbilical vein endothelial cells showing progressive wound healing up to 36 h. The 1% κCA-2%nanosilicate/VEGF shows higher wound closure in comparison to 1% κCA or 1% κCA/2% nanosilicates. (c) Quantitative data for wound closure for 1% κCA, 1% κCA/2% nanosilicate and 1% κCA/2% nanosilicate/VEGF was determined. Almost complete wound closure was observed in 1% κCA/2% nanosilicate/VEGF after 36 h in comparison to other groups. Positive control includes exposure of wound to 50 ng/mL VEGF. Rapid wound closure in hydrogel groups is attributed to the sustained release of VEGF and the accelerated migration of HUVECs.

healing in clinical settings [56]. Therefore, it was anticipated that sustained release of VEGF from κCA-nanosilicate hydrogel may lead to enhanced cell proliferation and wound healing.

To investigate the potential effect of VEGF release on wound healing, we encapsulated VEGF within κCA-nanosilicate hydrogels. The bioactivity of released VEGF was investigated using an *in vitro* scratch assay (Fig. 9a) and a migration assay. Bolus delivery of VEGF was used as control. In the scratch assay, a wound was created on a cell monolayer and subjected to VEGF release. No significant increase in wound closure was observed when the traumatized monolayer was subjected to control κCA and κCA-nanosilicates hydrogel without VEGF (Fig. 9b and c). The addition

of VEGF to 1% κCA-2% nanosilicate hydrogels showed higher wound closure. Similar results were obtained when observing the migration kinetics of HUVECs across a transwell membrane. Migration potential of HUVECS has been previously investigated [57]. HUVECs were seeded on top of a transwell membrane and placed in media containing VEGF encapsulated 1% κCA-2% nanosilicate, empty 1% κCA-2% nanosilicate and 1% κCA hydrogels. While there was negligible migration observed in 1% κCA after 24 h, VEGF released from κCA-nanosilicates nanocomposites allowed for enhanced migration of cells seeded on top of the transwell membrane as was evident from the prevalence of cells (Fig. 9d) observed on the bottom layer of the transwell. A sustained release of VEGF from nanocomposites can thus accelerate wound healing and ensure rapid wound closure by enhanced migration.

These results have shown that the κCA-nanosilicates hydrogels have clear advantages over the current available hemostats including improved mechanical and physiological stability, injectable characteristics, ability to dissociate over time, high biocompatibility, and accelerated clotting time. The presence of nanosilicates is the key in providing such a unique property combination to κCA based hydrogels. For example, κCA-nanosilicates hydrogels can be used for hemostatic purposes for internal injuries due to its shear-thinning characteristics, unlike commercially available hemostats [4–6] which are used for topical applications. Moreover, delivery of therapeutic biomolecules can stimulate wound healing ability which is currently lacking in commercially available hemostats.

4. Conclusion

In conclusion, κCA-nanosilicate hydrogels have great potential to accelerate clotting while simultaneously delivering therapeutics for wound healing. Nanosilicate integration in κCA hydrogels enhances the physiological stability, hemostatic, and wound healing potential of the nanocomposites. Through improved cellular interactions with the nanocomposite surface, wound healing responses may also be expedited. Further research into *in vivo* efficacy would be required to explore the full potential of these injectable hemostats. Sustained release of biomolecules from the nanocomposites with shear-thinning properties encourages further investigations into *in vivo* cell and therapeutic delivery. It is expected that the κCA-nanosilicate hydrogels could be used for reducing hemorrhage and wound healing.

Acknowledgement

M.P acknowledges financial support from SRM University for the Faculty Abroad Program (SRMU/IR/FAP/2015/001). A.K.G would like to acknowledge financial support from National Science Foundation (CBET 1705852), and National Institute of Health (EB023454). The manuscript was written through contributions of all authors. All authors have given approval to the final version of the manuscript.

References

[1] H.R. Champion, R.F. Bellamy, C.P. Roberts, A. Leppaniemi, A profile of combat injury, J. Trauma 54 (5 Suppl) (2003) S13–S19.
[2] M.N. Wente, J.A. Veit, C. Bassi, C. Dervenis, A. Fingerhut, D.J. Gouma, J.R. Izbicki, J.P. Neoptolemos, R.T. Padbury, M.G. Sarr, C.J. Yeo, M.W. Buchler, Postpancreatectomy hemorrhage (PPH): an International Study Group of Pancreatic Surgery (ISGPS) definition, Surgery 142 (1) (2007) 20–25.
[3] F. Feit, M.D. Voeltz, M.J. Attubato, A.M. Lincoff, D.P. Chew, J.A. Bittl, E.J. Topol, S. V. Manoukian, Predictors and impact of major hemorrhage on mortality following percutaneous coronary intervention from the REPLACE-2 Trial, Am. J. Cardiol. 100 (9) (2007) 1364–1369.
[4] H.E. Achneck, B. Sileshi, R.M. Jamiolkowski, D.M. Albala, M.L. Shapiro, J.H. Lawson, A comprehensive review of topical hemostatic agents: efficacy and recommendations for use, Ann. Surg. 251 (2) (2010) 217–228.
[5] H.B. Alam, D. Burris, J.A. DaCorta, P. Rhee, Hemorrhage control in the battlefield: role of new hemostatic agents, Mil. Med. 170 (1) (2005) 63–69.
[6] A.E. Pusateri, H.E. Modrow, R.A. Harris, J.B. Holcomb, J.R. Hess, R.H. Mosebar, T. J. Reid, J.H. Nelson, C.W. Goodwin Jr., G.M. Fitzpatrick, A.T. McManus, D.T. Zolock, J.L. Sondeen, R.L. Cornum, R.S. Martinez, Advanced hemostatic dressing development program: animal model selection criteria and results of a study of nine hemostatic dressings in a model of severe large venous hemorrhage and hepatic injury in Swine, J. Trauma 55 (3) (2003) 518–526.
[7] L. Yu, J. Ding, Injectable hydrogels as unique biomedical materials, Chem. Soc. Rev. 37 (8) (2008) 1473–1481.
[8] J.D. Kretlow, L. Klouda, A.G. Mikos, Injectable matrices and scaffolds for drug delivery in tissue engineering, Adv. Drug Delivery Rev. 59 (4–5) (2007) 263–273.
[9] M. Guvendiren, H.D. Lu, J.A. Burdick, Shear-thinning hydrogels for biomedical applications, Soft Matter. 8 (2) (2012) 260–272.
[10] T. Dvir, B.P. Timko, D.S. Kohane, R. Langer, Nanotechnological strategies for engineering complex tissues, Nat. Nanotechnol. 6 (1) (2011) 13–22.
[11] N.S. Satarkar, J.Z. Hilt, Hydrogel nanocomposites as remote-controlled biomaterials, Acta Biomater. 4 (1) (2008) 11–16.
[12] Y. Lu, A.A. Aimetti, R. Langer, Z. Gu, Bioresponsive materials, Nat. Rev. Mater. 2 (2016) 16075.
[13] J. Whitlow, S. Pacelli, A. Paul, Polymeric nanohybrids as a new class of therapeutic biotransporters, Macromol. Chem. Phys. 217 (11) (2016) 1245–1259.
[14] P. Kerativitayanan, J.K. Carrow, A.K. Gaharwar, Nanomaterials for engineering stem cell responses, Adv. Healthc. Mater. 4 (11) (2015) 1600–1627.
[15] P. Schexnailder, G. Schmidt, Nanocomposite polymer hydrogels, Colloid Polym. Sci. 287 (1) (2009) 1–11.
[16] A.K. Gaharwar, N.A. Peppas, A. Khademhosseini, Nanocomposite hydrogels for biomedical applications, Biotechnol. Bioeng. 111 (3) (2014) 441–453.
[17] L.M. Cross, A. Thakur, N.A. Jalili, M. Detamore, A.K. Gaharwar, Nanoengineered biomaterials for repair and regeneration of orthopedic tissue interfaces, Acta Biomater. 42 (2016) 2–17.
[18] D. Chimene, D.L. Alge, A.K. Gaharwar, Two-dimensional nanomaterials for biomedical applications: emerging trends and future prospects, Adv. Mater. 27 (45) (2015) 7261–7284 (Deerfield Beach, Fla.).
[19] B. Ruzicka, E. Zaccarelli, A fresh look at the Laponite phase diagram, Soft Matter. 7 (4) (2011) 1268–1286.
[20] D.W. Thompson, J.T. Butterworth, The nature of laponite and its aqueous dispersions, J. Colloid Interface Sci. 151 (1) (1992) 236–243.
[21] A.K. Gaharwar, S.M. Mihaila, A. Swami, A. Patel, S. Sant, R.L. Reis, A.P. Marques, M.E. Gomes, A. Khademhosseini, Bioactive silicate nanoplatelets for osteogenic differentiation of human mesenchymal stem cells, Adv. Mater. (Deerfield Beach, Fla.) 25 (24) (2013) 3329–3336.
[22] A.K. Gaharwar, S. Mukundan, E. Karaca, A. Dolatshahi-Pirouz, A. Patel, K. Rangarajan, S.M. Mihaila, G. Iviglia, H. Zhang, A. Khademhosseini, Nanoclay-enriched poly(varepsilon-caprolactone) electrospun scaffolds for osteogenic differentiation of human mesenchymal stem cells, Tissue Eng. Part A 20 (15–16) (2014) 2088–2101.
[23] O. Akhavan, E. Ghaderi, A. Akhavan, Size-dependent genotoxicity of graphene nanoplatelets in human stem cells, Biomaterials 33 (32) (2012) 8017–8025.
[24] J.I. Dawson, R.O. Oreffo, Clay: new opportunities for tissue regeneration and biomaterial design, Adv. Mater. 25 (30) (2013) 4069–4086 (Deerfield Beach, Fla.).
[25] M. Parani, G. Lokhande, A. Singh, A.K. Gaharwar, Engineered nanomaterials for infection control and healing acute and chronic wounds, ACS Appl. Mater. Interfaces 8 (16) (2016) 10049–10069.
[26] R. Angelini, E. Zaccarelli, F.A. de Melo Marques, M. Sztucki, A. Fluerasu, G. Ruocco, B. Ruzicka, Glass-glass transition during aging of a colloidal clay, Nat. Commun. 5 (2014) 4049.
[27] D. Bonn, S. Tanase, B. Abou, H. Tanaka, J. Meunier, Laponite: aging and shear rejuvenation of a colloidal glass, Phys. Rev. Lett. 89 (1) (2002) 015701.
[28] N. Bitinis, M. Hernandez, R. Verdejo, J.M. Kenny, M.A. Lopez-Manchado, Recent advances in clay/polymer nanocomposites, Adv. Mater. 23 (44) (2011) 5229–5236 (Deerfield Beach, Fla.).
[29] Q. Wang, J.L. Mynar, M. Yoshida, E. Lee, M. Lee, K. Okuro, K. Kinbara, T. Aida, High-water-content mouldable hydrogels by mixing clay and a dendritic molecular binder, Nature 463 (7279) (2010) 339–343.
[30] R. Waters, S. Pacelli, R. Maloney, I. Medhi, R.P. Ahmed, A. Paul, Stem cell secretome-rich nanoclay hydrogel: a dual action therapy for cardiovascular regeneration, Nanoscale 8 (14) (2016) 7371–7376.
[31] J.R. Xavier, T. Thakur, P. Desai, M.K. Jaiswal, N. Sears, E. Cosgriff-Hernandez, R. Kaunas, A.K. Gaharwar, Bioactive nanoengineered hydrogels for bone tissue engineering: a growth-factor-free approach, ACS Nano 9 (3) (2015) 3109–3118.
[32] J.I. Dawson, J.M. Kanczler, X.B. Yang, G.S. Attard, R.O. Oreffo, Clay gels for the delivery of regenerative microenvironments, Adv. Mater. 23 (29) (2011) 3304–3308 (Deerfield Beach, Fla.).
[33] A.K. Gaharwar, P.J. Schexnailder, B.P. Kline, G. Schmidt, Assessment of using Laponite® cross-linked poly(ethylene oxide) for controlled cell adhesion and mineralization, Acta Biomater. 7 (2) (2011) 568–577.

[34] A.K. Gaharwar, R.K. Avery, A. Assmann, A. Paul, G.H. McKinley, A. Khademhosseini, B.D. Olsen, Shear-thinning nanocomposite hydrogels for the treatment of hemorrhage, ACS Nano 8 (10) (2014) 9833–9842.
[35] A. Purwada, M.K. Jaiswal, H. Ahn, T. Nojima, D. Kitamura, A.K. Gaharwar, L. Cerchietti, A. Singh, Ex vivo engineered immune organoids for controlled germinal center reactions, Biomaterials 63 (2015) 24–34.
[36] A. Paul, V. Manoharan, D. Krafft, A. Assmann, J.A. Uquillas, S.R. Shin, A. Hasan, M.A. Hussain, A. Memic, A.K. Gaharwar, A. Khademhosseini, Nanoengineered biomimetic hydrogels for guiding human stem cell osteogenesis in three dimensional microenvironments, J. Mater. Chem. B 4 (20) (2016) 3544–3554.
[37] C.W. Peak, J. Stein, K.A. Gold, A.K. Gaharwar, Nanoengineered colloidal inks for 3D bioprinting, Langmuir (2017).
[38] S.N. Bhattacharyya, B. Manna, P. Ashbaugh, R. Coutinho, B. Kaufman, Differentiation of respiratory epithelium: the effects of retinoic acid and carcinogens on the expression of mucociliary vs. squamous phenotype, Inflammation 21 (2) (1997) 133–143.
[39] P.P. Kirsch, Carrageenan: a safe additive, Environ. Health Perspect. 110 (6) (2002) A288. author reply A288.
[40] T. Coviello, P. Matricardi, C. Marianecci, F. Alhaique, Polysaccharide hydrogels for modified release formulations, J. Control Release 119 (1) (2007) 5–24.
[41] I.S. Chronakis, J.L. Doublier, L. Piculell, Viscoelastic properties for kappa- and iota-carrageenan in aqueous NaI from the liquid-like to the solid-like behaviour, Int. J. Biol. Macromol. 28 (1) (2000) 1–14.
[42] A. Thakur, M.K. Jaiswal, C.W. Peak, J.K. Carrow, J. Gentry, A. Dolatshahi-Pirouz, A.K. Gaharwar, Injectable shear-thinning nanoengineered hydrogels for stem cell delivery, Nanoscale 8 (24) (2016) 12362–12372.
[43] A.K. Gaharwar, V. Kishore, C. Rivera, W. Bullock, C.J. Wu, O. Akkus, G. Schmidt, Physically crosslinked nanocomposites from silicate-crosslinked PEO: mechanical properties and osteogenic differentiation of human mesenchymal stem cells, Macromol. Biosci. 12 (6) (2012) 779–793.
[44] J.D. Stroncek, Y. Xue, N. Haque, J.H. Lawson, W.M. Reichert, In vitro functional testing of endothelial progenitor cells that overexpress thrombomodulin, Tissue Eng. Part A 17 (15–16) (2011) 2091–2100.
[45] E.W. Davie, K. Fujikawa, W. Kisiel, The coagulation cascade: initiation, maintenance, and regulation, Biochemistry 30 (43) (1991) 10363–10370.
[46] K. Naito, K. Fujikawa, Activation of human blood coagulation factor XI independent of factor XII Factor XI is activated by thrombin and factor XIa in the presence of negatively charged surfaces, J. Biol. Chem. 266 (12) (1991) 7353–7358.
[47] G.D. Yancopoulos, S. Davis, N.W. Gale, J.S. Rudge, S.J. Wiegand, J. Holash, Vascular-specific growth factors and blood vessel formation, Nature 407 (6801) (2000) 242–248.
[48] S. Barrientos, O. Stojadinovic, M.S. Golinko, H. Brem, M. Tomic-Canic, Growth factors and cytokines in wound healing, Wound Repair Regen. 16 (5) (2008) 585–601.
[49] D.E. Discher, D.J. Mooney, P.W. Zandstra, Growth factors, matrices, and forces combine and control stem cells, Science 324 (5935) (2009) 1673–1677.
[50] P.S. Briquez, J.A. Hubbell, M.M. Martino, Extracellular matrix-inspired growth factor delivery systems for skin wound healing, Adv. Wound Care (New Rochelle) 4 (8) (2015) 479–489.
[51] N.A. Jalili, M. Muscarello, A.K. Gaharwar, Nanoengineered thermoresponsive magnetic hydrogels for biomedical applications, Bioeng. Transl. Med. 1 (3) (2016) 297–305.
[52] J. Meissner, A. Prause, B. Bharti, G.H. Findenegg, Characterization of protein adsorption onto silica nanoparticles: influence of pH and ionic strength, Colloid Polym. Sci. 293 (11) (2015) 3381–3391.
[53] P. Bao, A. Kodra, M. Tomic-Canic, M.S. Golinko, H.P. Ehrlich, H. Brem, The role of vascular endothelial growth factor in wound healing, J. Surg. Res. 153 (2) (2009) 347–358.
[54] K.E. Johnson, T.A. Wilgus, Vascular endothelial growth factor and angiogenesis in the regulation of cutaneous wound repair, Adv. Wound Care (New Rochelle) 3 (10) (2014) 647–661.
[55] G.C. Gurtner, S. Werner, Y. Barrandon, M.T. Longaker, Wound repair and regeneration, Nature 453 (7193) (2008) 314–321.
[56] W.J. Jeffcoate, S.Y. Chipchase, P. Ince, F.L. Game, Assessing the outcome of the management of diabetic foot ulcers using ulcer-related and person-related measures, Diabetes Care 29 (8) (2006) 1784–1787.
[57] O. Naoko, T. Hiroyuki, T. Yasuhiko, Human umbilical vein endothelial cells migration in matrigel by the, 5 (4) (2015), 9.